

Minimum weighted norm interpolation of seismic records

Bin Liu¹ and Mauricio D. Sacchi¹

ABSTRACT

In seismic data processing, we often need to interpolate and extrapolate data at missing spatial locations. The reconstruction problem can be posed as an inverse problem where, from inadequate and incomplete data, we attempt to reconstruct the seismic wavefield at locations where measurements were not acquired.

We propose a wavefield reconstruction scheme for spatially band-limited signals. The method entails solving an inverse problem where a wavenumber-domain regularization term is included. The regularization term constrains the solution to be spatially band-limited and imposes a prior spectral shape. The numerical algorithm is quite efficient since the method of conjugate gradients in conjunction with fast matrix–vector multiplications, implemented via the fast Fourier transform (FFT), is adopted. The algorithm can be used to perform multi-dimensional reconstruction in any spatial domain.

INTRODUCTION

The seismic data reconstruction problem arises in many processing steps that require regular sampling. Different methods have been proposed: for example, prediction error filtering interpolation (Spitz, 1991; Claerbout, 1992), wave equation-based interpolation (Ronen, 1987), and Fourier reconstruction (Sacchi and Ulrych, 1996; Cary, 1997; Hindriks et al., 1997; Sacchi et al., 1998; Duijndam et al., 1999; Zwartjes and Duijndam, 2000). Among those methods, Fourier-based reconstruction starts by posing the interpolation/extrapolation problem as an inverse problem where, from inadequate and incomplete data, one attempts to recover the discrete Fourier transform of the seismic wavefield.

Inverse problems are known to be ill posed and require regularization to obtain unique and stable solutions. Criteria to choose a suitable regularization strategy in the context of interpolation and extrapolation are discussed by several re-

searchers (Cabrera and Parks, 1991; Sacchi and Ulrych, 1996; Hindriks et al., 1997; Sacchi et al., 1998; Duijndam et al., 1999; Zwartjes and Duijndam, 2000). For example, minimum norm spectral regularization can be used when we assume that seismic data are band-limited in the spatial wavenumber domain (Duijndam et al., 1999). Similarly, a regularization derived using the Cauchy criterion can be used to obtain a high-resolution (sparse) discrete Fourier transform that can synthesize the data at new spatial positions (Sacchi and Ulrych, 1996; Sacchi et al., 1998; Zwartjes and Duijndam, 2000). The sparse spectrum assumption is appropriate for data that consist of a superposition of a few plane waves (Sacchi and Ulrych, 1996). Processing the input data in windows is often necessary when assuming a sparse spectrum model. However, an interpolation scheme that operates on small windows might not be optimal for multidimensional data reconstruction in the presence of large portions of missing data.

In this paper we introduce a minimum weighted norm interpolation (MWNI) algorithm to perform multidimensional reconstruction of seismic wavefields. In particular, we minimize a wavenumber weighted norm that lets us incorporate a prior spectral signature of the unknown wavefield. The procedure is an extension of the adaptive frequency-domain weighted norm scheme proposed by Cabrera and Parks (1991) to extrapolate time series. Our work adapts the Cabrera and Parks (1991) method to the seismic data reconstruction problem. We also extend the problem to the multidimensional case. In addition, we avoid direct inversion methods and opt for a more efficient optimization scheme based on the method of conjugate gradients with preconditioning.

Numerical examples with synthetic and field data demonstrate the merits of the proposed interpolation scheme.

INTERPOLATION OF BAND-LIMITED DATA

Basic definitions

We start our analysis with a 1D interpolation problem. The extension to higher dimensions is proposed in the next section. By 1D interpolation, we understand interpolation in the f - x domain along the spatial dimension x . In other words, a seismic

Manuscript received by the Editor January 22, 2003; revised manuscript received May 16, 2004.

¹University of Alberta, Institute for Geophysical Research and Department of Physics, Edmonton, Alberta, Canada, T6G 2J1. E-mail: binliu@phys.ualberta.ca; sacchi@phys.ualberta.ca.

© 2004 Society of Exploration Geophysicists. All rights reserved.

gather in the t - x domain is first transformed to the frequency domain and then interpolation is carried out along the spatial dimension x for each temporal frequency f .

We denote \mathbf{x} as the length- M vector of data sampled on a regular grid $x_1, x_2, x_3, \dots, x_M$. The observations are given by the elements of the vector $\mathbf{y} = [x_{n(1)}, x_{n(2)}, x_{n(3)}, \dots, x_{n(N)}]^T$, where the set $\mathcal{N} = \{n(1), n(2), n(3), \dots, n(N)\}$ indicates the position of the known samples or observations. We now define the sampling matrix \mathbf{T} with elements $T_{i,j} = \delta_{n(i),j}$, where δ indicates the Kronecker operator. It is quite simple to show that the complete data and the observations are connected by the following linear system:

$$\mathbf{y} = \mathbf{T}\mathbf{x}. \quad (1)$$

For example, let us assume the complete data set consists of $M = 5$ consecutive samples, or $\mathbf{x} = [x_1, x_2, x_3, x_4, x_5]^T$; the observations (available data) are given by samples at positions $\mathcal{N} = \{2, 3, 5\}$, or $\mathbf{y} = [x_2, x_3, x_5]^T$. Then equation 1 becomes

$$\begin{pmatrix} x_2 \\ x_3 \\ x_5 \end{pmatrix} = \begin{pmatrix} 0 & 1 & 0 & 0 & 0 \\ 0 & 0 & 1 & 0 & 0 \\ 0 & 0 & 0 & 0 & 1 \end{pmatrix} \begin{pmatrix} x_1 \\ x_2 \\ x_3 \\ x_4 \\ x_5 \end{pmatrix}. \quad (2)$$

Note that the sampling operator \mathbf{T} has the following property:

$$\mathbf{T}\mathbf{T}^T = \mathbf{I}_N, \quad (3)$$

where \mathbf{I}_N denotes the $N \times N$ identity matrix. In addition, $\mathbf{T}^T\mathbf{T} \neq \mathbf{I}_M$. We also define the discrete Fourier transform (DFT) and the inverse discrete Fourier transform (IDFT) respectively, as follows:

$$X_k = \frac{1}{\sqrt{M}} \sum_{m=1}^M x_m e^{-i2\pi(m-1)(k-1)/M}, \quad k = 1, \dots, M, \quad (4)$$

$$x_m = \frac{1}{\sqrt{M}} \sum_{k=1}^M X_k e^{i2\pi(m-1)(k-1)/M}, \quad m = 1, \dots, M. \quad (5)$$

We use the following compact notation for the DFT and IDFT, respectively:

$$\mathbf{X} = \mathbf{F}\mathbf{x}, \quad (6)$$

$$\mathbf{x} = \mathbf{F}^H\mathbf{X}, \quad (7)$$

where the superscript H denotes the complex conjugate transpose. Notice that \mathbf{F} is the DFT unitary matrix whose inverse is given by $\mathbf{F}^{-1} = \mathbf{F}^H$.

Minimum weighted norm inversion of the sampling operator

The signal reconstruction or interpolation problem given by equation 1 entails solving an underdetermined system of equations (more unknowns than observations). It is clear that the problem does not have a unique solution. In general, one way

of solving this type of problem is by restricting the class of solutions through providing suitable prior information.

Let us continue the analysis by saying that among all the possible solutions, we seek a solution that minimizes a model norm. In the absence of errors, the inversion can be reduced to solving the following constrained minimization problem:

$$\begin{aligned} &\text{Minimize} \quad \|\mathbf{x}\|_{\mathcal{W}}^2 \\ &\text{Subject to} \quad \mathbf{T}\mathbf{x} = \mathbf{y}, \end{aligned}$$

where $\|\cdot\|_{\mathcal{W}}$ indicates a weighted norm. Following Cabrera and Parks (1991), we select the following wavenumber-domain norm:

$$\|\mathbf{x}\|_{\mathcal{W}}^2 = \sum_{k \in \mathcal{K}} \frac{X_k^* X_k}{P_k^2}, \quad (8)$$

where P_k^2 are spectral domain weights with support and shape similar to those of the signal to interpolate. The set of indexes \mathcal{K} indicates the region of spectral support of the signal. It is understood that $P_k \neq 0$ for $k \in \mathcal{K}$. The coefficient P_k represents the spectral power at wavenumber index k .

We now introduce a diagonal matrix Λ with elements given by

$$\Lambda_k = \begin{cases} P_k^2, & k \in \mathcal{K} \\ 0, & k \notin \mathcal{K} \end{cases}. \quad (9)$$

Similarly, we define the pseudoinverse of the diagonal matrix Λ , as the matrix Λ^\dagger with elements given by

$$\Lambda_k^\dagger = \begin{cases} P_k^{-2}, & k \in \mathcal{K} \\ 0, & k \notin \mathcal{K} \end{cases}. \quad (10)$$

The wavenumber-domain norm can now be expressed as

$$\|\mathbf{x}\|_{\mathcal{W}}^2 = \mathbf{X}^H \Lambda^\dagger \mathbf{X}. \quad (11)$$

After combining equations 7 and 8, we arrive at the following expression:

$$\begin{aligned} \|\mathbf{x}\|_{\mathcal{W}}^2 &= \mathbf{x}^H \mathbf{F}^H \Lambda^\dagger \mathbf{F} \mathbf{x} \\ &= \mathbf{x}^H \mathbf{Q}^\dagger \mathbf{x}, \end{aligned} \quad (12)$$

where $\mathbf{Q}^\dagger = \mathbf{F}^H \Lambda^\dagger \mathbf{F}$ is a circulant matrix (Strang, 1986). Similarly, we define the circulant matrix $\mathbf{Q} = \mathbf{F}^H \Lambda \mathbf{F}$. Notice that both \mathbf{Q} and \mathbf{Q}^\dagger are band-limiting operators. In other words, they annihilate any spectral component $k \notin \mathcal{K}$.

The minimum norm solution is found by minimizing the following cost function:

$$J = \mathbf{b}^T (\mathbf{T}\mathbf{x} - \mathbf{y}) + \|\mathbf{x}\|_{\mathcal{W}}^2.$$

In the above equation, \mathbf{b} denotes the vector of Lagrange multipliers. Minimizing J with respect to \mathbf{x} subject to $\mathbf{T}\mathbf{x} - \mathbf{y} = \mathbf{0}$ leads to the following solution:

$$\hat{\mathbf{x}} = \mathbf{Q}\mathbf{T}^T (\mathbf{T}\mathbf{Q}\mathbf{T}^T)^{-1} \mathbf{y}. \quad (13)$$

In the previous derivation we assume that the matrix $\mathbf{T}\mathbf{Q}\mathbf{T}^T$ is invertible. If this is not the case, the inverse can be replaced by the Moore-Penrose pseudoinverse (Cabrera and Parks, 1991).

The above solution is designated as MWNI. We reserve the name minimum norm interpolation (MNI) for the case where \mathbf{Q} is a band-pass filter with spectral weights $P_k^2 = 1, k \in \mathcal{K}$. In

other words, we constraint the solution to the class of band-limited signals with spectral components in $k \in \mathcal{K}$, and we make no attempt to impose a prior spectral shape.

Let us consider the case when \mathbf{Q} is an all-pass filtering matrix with DFT coefficients $\Lambda_k = 1$ for $k = 1, \dots, M$. In this case, $\Lambda = \mathbf{I}$, and after invoking the orthonormality of the DFT operator we obtain the following expression:

$$\hat{\mathbf{x}} = \mathbf{T}^T (\mathbf{T}\mathbf{T}^T)^{-1} \mathbf{y} = \mathbf{T}^T \mathbf{y}. \quad (14)$$

In the *toy* example provided by equation 2, the minimum norm solution becomes

$$\hat{\mathbf{x}} = \mathbf{T}^T \mathbf{y} = \begin{pmatrix} 0 \\ x_2 \\ x_3 \\ 0 \\ x_5 \end{pmatrix}. \quad (15)$$

In other words, missing samples are filled in with zeros.

Inversion of \mathbf{T} in the presence of noise

When the observations contain additive noise rather than trying to fit exactly all of the observations, we attempt to fit the observations in the least-squares sense. In this case we minimize a cost function that combines a data misfit function in conjunction with the model norm:

$$J = \|\mathbf{T}\mathbf{x} - \mathbf{y}\|^2 + \rho^2 \|\mathbf{x}\|_{\mathcal{W}}^2, \quad (16)$$

where ρ^2 is the trade-off parameter of the problem. Notice that minimizing J is equivalent to finding the least-squares solution of the following overdetermined system of equations:

$$\begin{pmatrix} \mathbf{T} \\ \rho \mathbf{W} \end{pmatrix} \mathbf{x} \approx \begin{pmatrix} \mathbf{y} \\ \mathbf{0} \end{pmatrix}, \quad (17)$$

where, according to our previous definitions, the matrix of weights \mathbf{W} is given by

$$\mathbf{W} = \Lambda^{\dagger 1/2} \mathbf{F}. \quad (18)$$

Unfortunately, the augmented matrix of the problem is rank deficient; therefore, equation 17 does not have a unique solution. The latter can be solved by choosing, among all possible least-squares solutions, the one with the minimum Euclidean norm. This can be done with the aid of the singular value decomposition (SVD) of the augmented matrix. Alternatively, we can use the method of conjugate gradients. For rank-deficient problems, the solution to which the conjugate gradient method converges depends upon the initial approximation adopted. If the initial approximation is chosen to be $\mathbf{x} = \mathbf{0}$, then the conjugate gradient converges to the minimum-norm least-squares solution (Hestenes, 1975). One advantage of using the conjugate gradient method is that the computational cost of the algorithm heavily depends on matrix-vector multiplications. These operations can be performed efficiently using the fast Fourier transform (FFT).

In our numerical implementation, equation 17 is modified with the following change of variable: $\mathbf{z} = \mathbf{W}\mathbf{x}$. The augmented

system becomes

$$\begin{pmatrix} \mathbf{T}\mathbf{W}^\dagger \\ \rho \mathbf{I} \end{pmatrix} \mathbf{z} \approx \begin{pmatrix} \mathbf{y} \\ \mathbf{0} \end{pmatrix}. \quad (19)$$

The trade-off parameter can be set to $\rho = 0$, and the number of iterations in the conjugate gradient method plays the role of regularization parameter (Hansen, 1998). We end up solving $\mathbf{T}\mathbf{W}^\dagger \mathbf{z} \approx \mathbf{y}$ and stopping the algorithm when a maximum number of iterations is reached or a desired misfit is achieved: $\|\mathbf{T}\mathbf{x} - \mathbf{y}\| < \text{tolerance}$, $\text{tolerance} = 10^{-3} - 10^{-5}$. We find that the conjugate gradient method often converges in less than 15 iterations.

At this point a few comments are in order. The transition from equation 17 to equation 19 is only valid for a full-rank matrix \mathbf{W} . The fact that we are solving for a band-limited solution ($k \in \mathcal{K}$), however, permits us to claim that solving equation 19 is equivalent to solving equation 17 (Nichols, 1997).

It is important to clarify that the proposed algorithm differs from the one proposed by Sacchi and Ulrych (1996) to invert the coefficient of the DFT using sparseness constraints. First of all, our algorithm does not assume a sparse distribution of spectral amplitudes. The latter is only valid for estimating the DFT of a process that consists of a finite number of spectral lines (Sacchi et al. 1998). To be more specific, the high-resolution Fourier transform (HRFT) proposed by Sacchi and Ulrych (1996) utilizes a Cauchy regularization criterion of the form

$$\|\mathbf{x}\|_c = \sum_k \ln \left(1 + \frac{X_k X_k^*}{\sigma_c^2} \right), \quad (20)$$

where σ_c is the scale parameter of the Cauchy norm.

Notice the difference between the above norm (equation 20) and the norm utilized in this paper (equation 8). It is very important to stress that the Cauchy criterion was proposed as a means of estimating sparse (high-resolution) spectral estimators for waveforms that can be approximated by plane waves. In this case, a sparse spectrum is the appropriate model for data that consist of a superposition of a few plane waves. In this paper, however, we propose a more general norm that is capable of handling nonsparse spectral models. The new approach is particularly relevant for multidimensional seismic data, where the common assumption of a local superposition of a few plane waves is suboptimal. Windowing can be used to validate the nonsparse spectral model. However, we prefer an alternative procedure where sparseness is not invoked. It is true that both MWNI and HRFT lead to very similar algorithms. However, in HRFT the amplitude of the Fourier transform $|X_k|^2$ plays the role of a data-dependent diagonal regularization matrix [see equation 19 in Sacchi and Ulrych (1996)]. In the MWNI formulation, on the other hand, the matrix of weights is derived from the power spectrum of the data using a non-parametric spectral estimator. In the next section we propose a procedure to estimate the power spectrum of the unknown data.

It is also important to clarify that the present work does not attempt to invert the nonuniform DFT (Hindriks et al., 1997). Our implementation utilizes FFTs; therefore, an important gain in efficiency is achieved when interpolating data that depend on more than one spatial dimension.

Adaptive estimation of the weighting operator

To obtain the matrix of weights \mathbf{W} , in practice one should know the power spectrum of the complete data \mathbf{x} . Unfortunately, the complete data \mathbf{x} are the unknowns of our problem. The latter can be overcome by defining an iterative scheme to bootstrap the spectral weights from the data. Our numerical implementation uses the smooth periodogram of the data (Bingham et al., 1967):

$$P_k^2 = \begin{cases} \sum_{l=-L}^L w_l |X_{k-l}|^2, & k \in \mathcal{K}, \\ 0, & k \notin \mathcal{K}, \end{cases} \quad (21)$$

where w_l is a smoothing window of length $2L + 1$. We initialize the algorithm with the band-limiting operator with spectral weights $P_k^2 = 1, k \in \mathcal{K}$; we solve for \mathbf{x} and use the solution to recompute P_k^2 using equation 21.

Alternatively, it is possible to adopt a noniterative strategy similar to the one proposed by Herrmann et al. (2000) to compute the high-resolution parabolic Radon transform. The method is well documented in Hugonnet et al. (2001). The power spectrum P_k^2 required to interpolate spatial data at a temporal frequency f can be estimated from the already interpolated data at frequency $f - \Delta f$. Such a scheme is often effective in dealing with situations where the data exhibit a mild degree of spatial aliasing at high frequencies.

In particular, in situations with aliasing produced by non-conflicting dips, the weighting operator computed from the nonaliased low frequencies attenuates the aliasing that might arise at high frequencies. Clearly, the assumption at the time of adopting such scheme is that the power spectrum of the data at frequency $f - \Delta f$ is similar in shape to the power spectrum of the data at frequency f . This assumption is often valid when Δf is small. This is achieved, in general, by padding the data with zeros before applying the Fourier transform.

1D reconstruction examples

Reconstruction along one spatial coordinate is illustrated with a synthetic shot gather. Figure 1a shows a complete shot gather with a small amount of random noise. The synthetic data were modeled with a ray-tracing algorithm for laterally invariant media; the amplitude variation with offset (AVO) effect is added using Shuey's equation (Shuey, 1987). A total of 18 traces were removed from the original data, including some near-offset traces (Figure 1b). The incomplete data set is used as input for our reconstruction algorithm. The data set is first transformed to the temporal frequency domain. The reconstruction is then performed along the spatial coordinate (receiver position) for each temporal frequency. Figure 1c shows the reconstruction using the MWNI algorithm. The modified periodogram (equation 21) is used to iteratively estimate the matrix of weights. The reconstruction error is portrayed in Figure 1d.

For comparison, we also tried to reconstruct the data using the HRFT algorithm (Sacchi and Ulrych, 1996) and the minimum norm interpolation (MNI) algorithm. Note that in the HRFT example we used all of the traces that compose the synthetic shot gather (no attempt at data windowing was made). The MNI algorithm had difficulties when interpolating large gaps. The MWNI and HRFT algorithms both managed to

retrieve comparable interpolation results. However, numerical experiments have shown that the HRFT tends to produce spectral models that are too sparse and tends to produce large interpolation errors when dealing with data that do not fit the sparse spectral model (seismic events with curvature in $t-x$).

We also compare the reconstructed power spectrum at the temporal frequency component $f = 15.6$ Hz for the MWNI, HRFT, and MNI methods. Figure 2a shows the power spectrum of the reconstructed data using the MWNI method. Figure 2b portrays the power spectrum of the reconstructed data using the HRFT approach. The spectrum of the reconstructed data using the MNI method is portrayed in Figure 2c. Finally, the power spectrum of the true (complete) data is displayed in Figure 2d. Notice the good agreement of the spectral signatures of the interpolated and original data in Figures 2a and 2d. The spectrum obtained using the HRFT approach (Figure 2b) is better than the spectrum obtained using the MNI method (Figure 2c); however, as we have already mentioned,

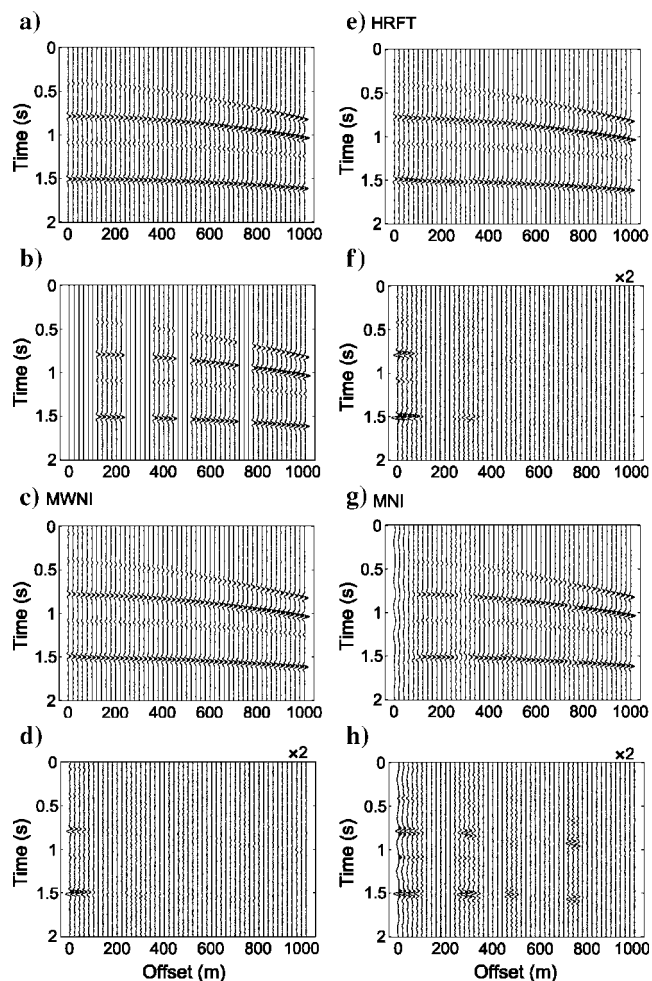


Figure 1. (a) Original synthetic shot gather. (b) Incomplete shot gather obtained by removing 18 traces from the complete shot gather in (a). (c) Reconstruction using the MWNI algorithm. (d) Reconstruction error after interpolation with the MWNI method. (e) Reconstruction using the HRFT approach. (f) Reconstruction error after interpolation with the HRFT method. (g) Reconstruction using MNI. (h) Reconstruction error after interpolation with the MNI method. Error panels (d), (f), and (h) are multiplied by two to better depict differences.

interpolation with the HRFT approach tends to produce spectral estimates that are too sparse.

It is important to stress that for the MNI method we have used a frequency-dependent bandwidth. The maximum wavenumber at frequency f is estimated using the formula $k_{max} = f/v_{min}$, where v_{min} is the minimum apparent velocity of the data (Duijndam et al. 1999).

The interpolation of a real marine shot gather using the MWNI method is portrayed in Figure 3. Figure 3a shows the marine shot gather before interpolation. The interpolated data at twice the original sample rate is portrayed in Figure 3b. In this example, we have determined the spectral weights using the noniterative scheme described above. The noniterative scheme is much faster than the iterative approach. Therefore, the noniterative scheme is utilized in all of the remaining examples. Our tests show minimal difference between these two approaches.

2D SPATIAL INTERPOLATION

The 1D interpolation algorithm proposed in the previous section can be extended to two dimensions by using Kroneker products (Davis, 1979; Jain and Ranganath, 1981). First, we denote the lexicographic ordering of the elements of the 2D $M_u \times M_v$ complete data matrix along two arbitrary spatial dimensions u and v as the vector \mathbf{x} . Similarly, the observations (obtained after binning the data) can also be organized in a data vector \mathbf{y} . Again, we can relate the complete data in the regular grid to the observations with a simple mapping of the form $\mathbf{T}\mathbf{x} = \mathbf{y}$. The band-limiting operator \mathbf{W} is now defined in terms of the following operations:

$$\mathbf{W} = \Lambda^{\dagger 1/2}(\mathbf{F}_u \otimes \mathbf{F}_v), \quad (22)$$

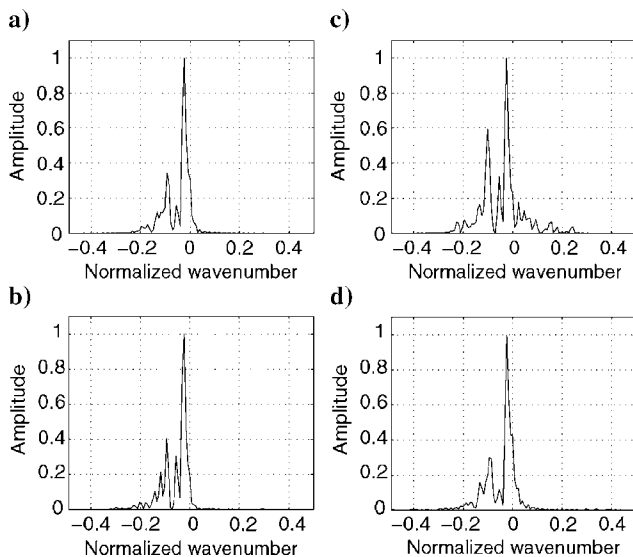


Figure 2. Power spectra at frequency component $f = 15.6$ Hz for data shown in Figure 1. (a) Power spectrum of the reconstructed data using the MWNI method. (b) Power spectrum of the reconstructed data using the HRFT approach. (c) Power spectrum of the reconstructed data using the MNI method. (d) Power spectrum of the original (complete) data.

where \mathbf{F}_u and \mathbf{F}_v denote 1D DFTs along dimensions u and v , respectively. The Kroneker product $\mathbf{F}_u \otimes \mathbf{F}_v$ is the 2D DFT matrix operating on the vectorized data. Similarly, the 2D power spectrum of the data (in vectorized form) is distributed along the diagonal of Λ . With these new definitions, we can easily extend the conjugate gradient algorithm discussed in a preceding section to the 2D case. It is clear that this scheme can be extended to interpolate three or more spatial variables simultaneously.

Interpolation in source-receiver coordinates

The effectiveness of the 2D MWNI method is first demonstrated using the Marmousi data set. The spatial coordinates to interpolate are source and receiver positions. It is important to stress that similar results could be obtained by interpolating in midpoint-offset coordinates. The input data are a subset of the Marmousi data set that consists of 24 shots with 96 receiver positions per shot. The original shots and receivers were sampled every 25 m. We simulate a survey with shot and receiver intervals of 75 m. In other words, 8 shots with 36 receivers per shot were extracted from the data and input to our reconstruction algorithm.

Figure 4 shows the shot-receiver distribution of the observations and positions to reconstruct. The original data, the input data, the reconstructed data, and the reconstruction error for three shots in the survey (source positions: 3075, 3100, and

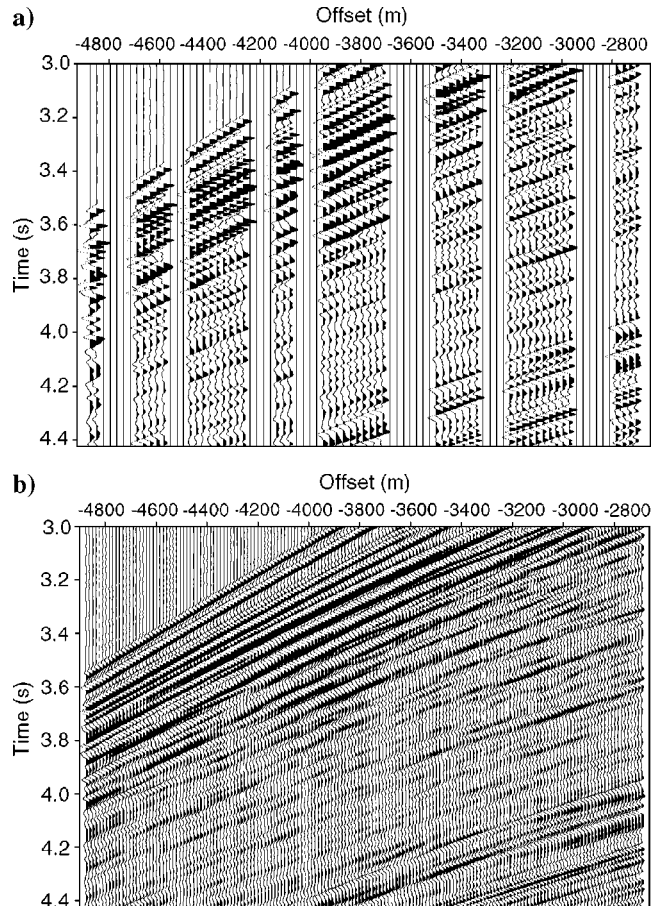


Figure 3. (a) Incomplete data from a real marine shot gather. (b) Interpolated data using the MWNI method.

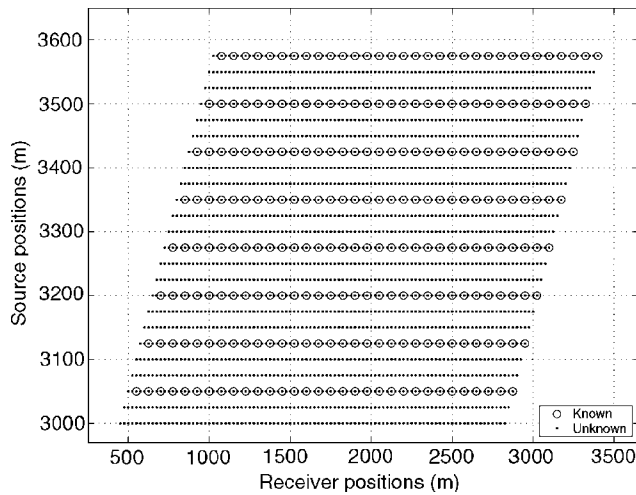


Figure 4. Source and receiver location map for a subset of the Marmousi model.

3125 m) are shown in Figures 5a–d, respectively. The f - k spectra of the original, decimated, and reconstructed shot gathers at 3125 m are shown in Figures 6a–c, respectively.

3D poststack seismic data reconstruction

We also illustrate the reconstruction of a real 3D poststack data cube using the 2D MWNI algorithm. In this case the interpolation is carried out along the inline and crossline coordinates. Figure 7a shows a complete 3D poststack data cube that consists of 51 inlines and 31 crosslines. The decimated poststack data cube (Figure 7b) is obtained by removing every second trace along both the inline and crossline directions. The incomplete data cube is used as input to the MWNI reconstruction algorithm. Figure 7c shows the cube after reconstruction. Detailed panels showing the true complete data, the reconstructed data, and the reconstruction error for inline 39 and crossline 19 are provided in Figures 8 and 9, respectively. Notice that the proposed interpolation has also attenuated the random noise. The degree of noise attenuation versus fidelity

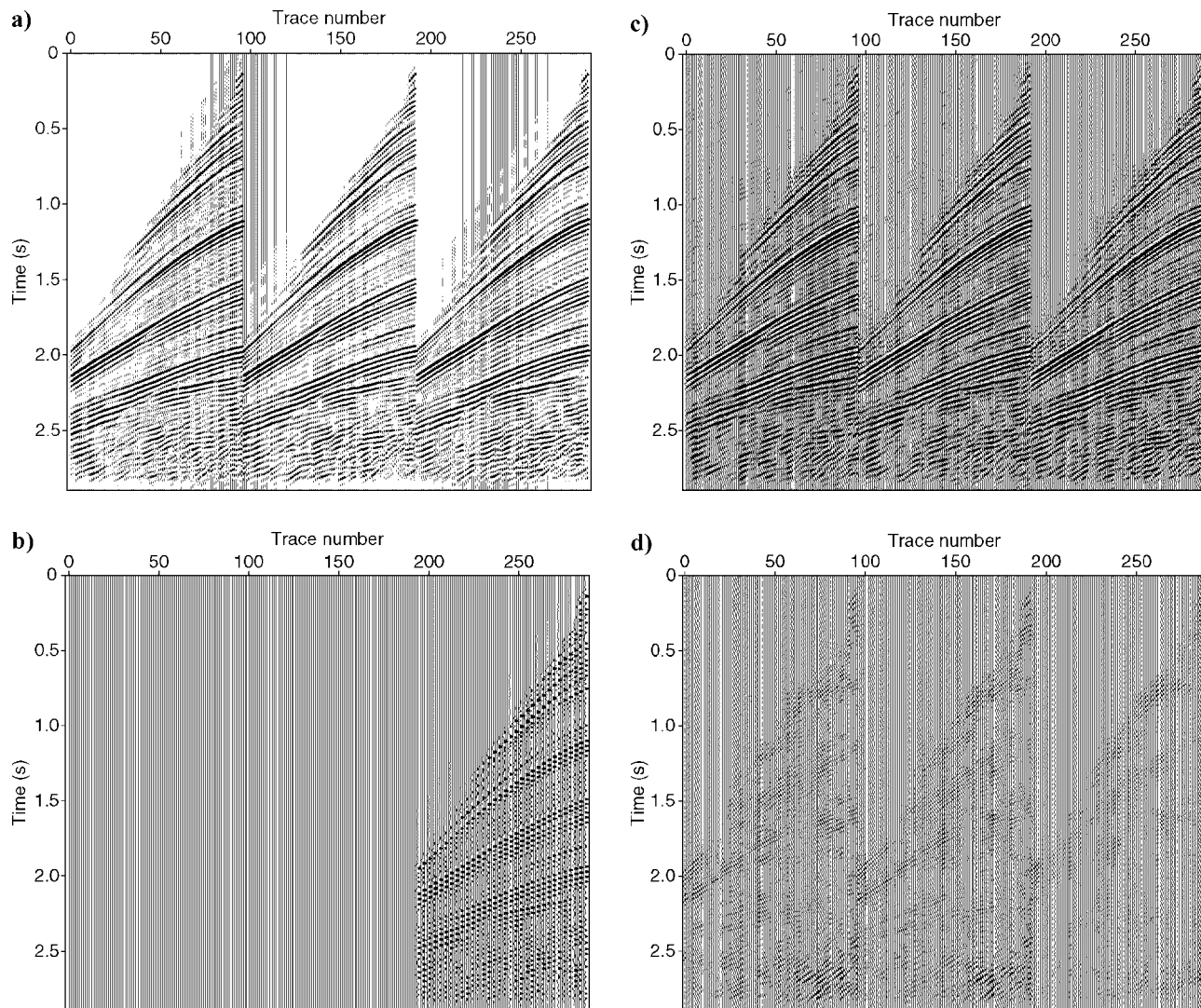


Figure 5. (a) Three shots extracted from the Marmousi data set. (b) Decimated shots. (c) Reconstructed data using the 2D MWNI algorithm. (d) Error panel.

of the reconstruction is regulated by the number of iterations of the conjugate gradient solver.

CONCLUSIONS

In this paper, we have formulated a band-limited data reconstruction algorithm that can incorporate prior spectral weights to control the bandwidth and the spectral shape of the reconstructed data. The MWNI method has been shown to perform better than standard MNI when dealing with large data gaps.

We have also discussed the differences between MWNI and data reconstruction via HRFT (Sacchi and Ulrych, 1996). The MWNI method avoids the sparse spectrum assumption; this is an important advantage when processing seismic data that do not satisfy the sparse spectrum model. It is clear that the sparse spectrum assumption is only valid for data that consist of a few

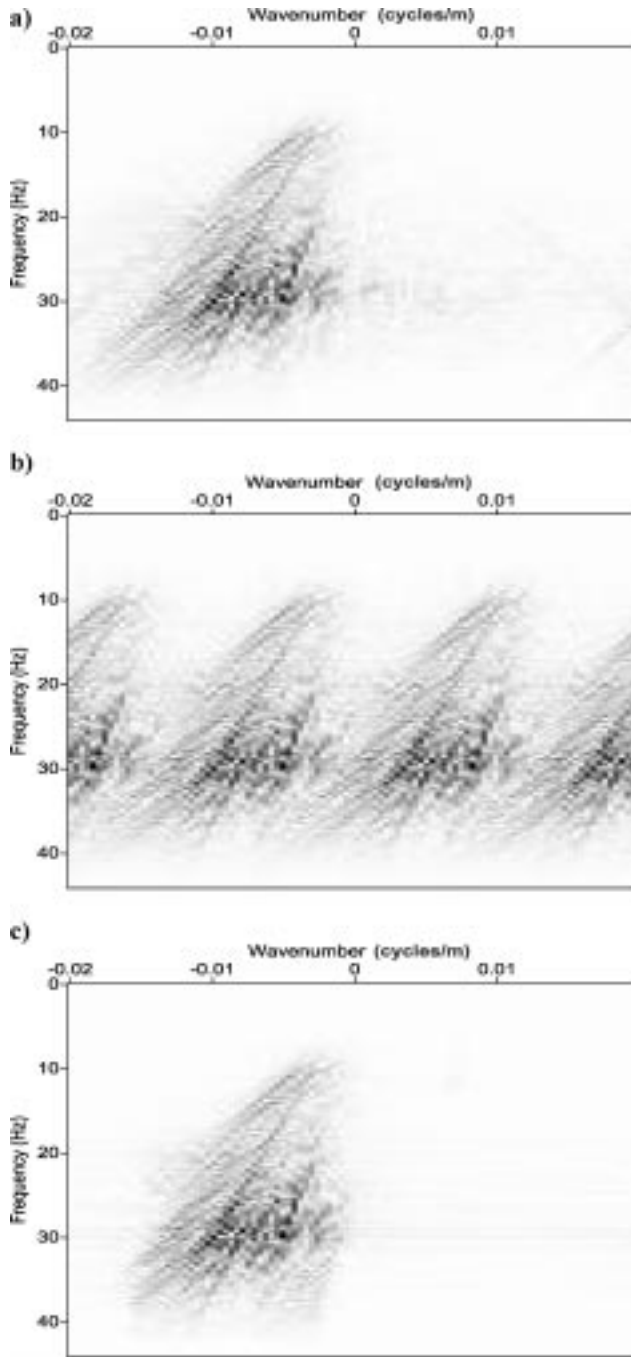


Figure 6. (a) The $f-k$ spectrum of the original shot gather at 3125 m. (b) The $f-k$ spectrum of the same shot gather after decimation. (c) The $f-k$ spectrum of the same shot gather after interpolation.

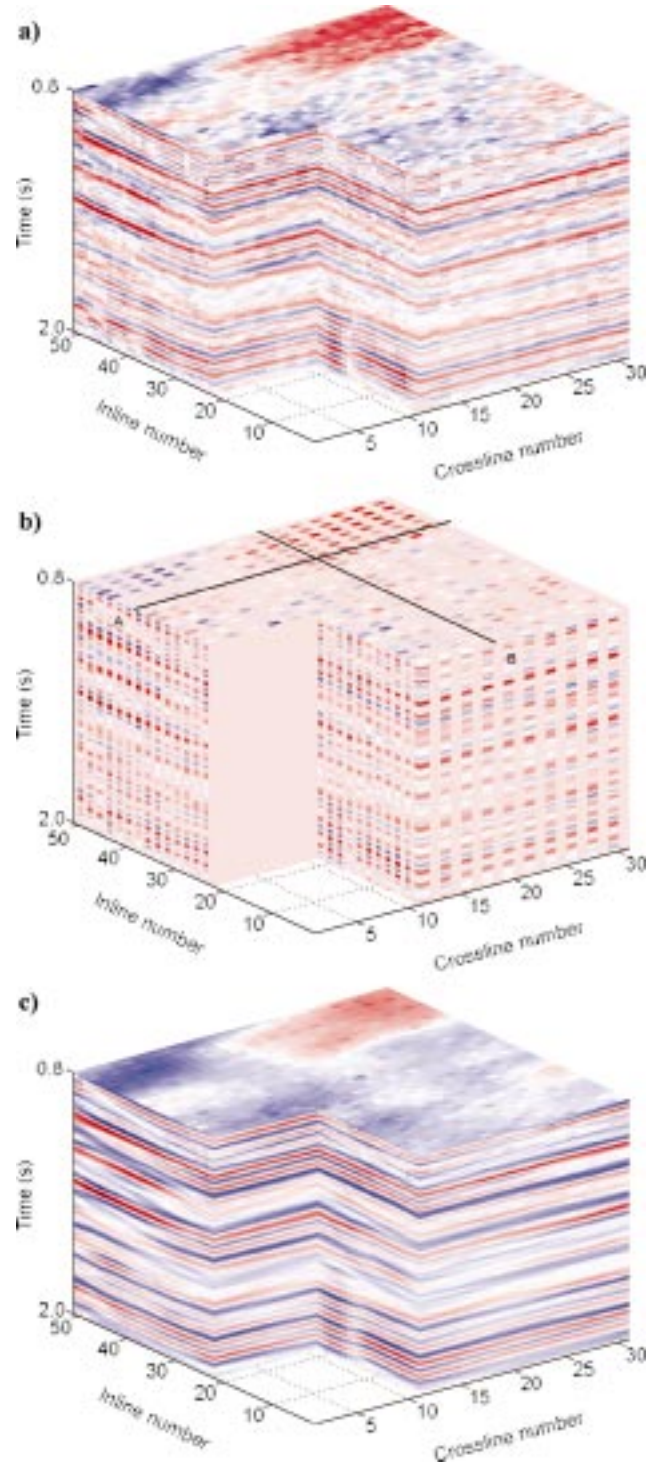


Figure 7. (a) A complete 3D poststack data cube. (b) Decimated cube; every second line is removed. (c) Reconstructed cube using the MWNI method.

plane waves (linear events in $t-x$). This is a valid assumption when reconstructing data in small windows. However, an interpolation scheme that operates on small windows might not be optimal for data reconstruction in the presence of large gaps.

In the presence of additive noise, a least-squares minimum weighted norm solution can be computed efficiently using the

method of conjugate gradients. It is important to stress that the computational cost of the conjugate gradient method heavily depends on matrix-vector multiplications. These operations can be implemented efficiently using the FFT. Additional efficiency can be obtained by truncating the number of conjugate gradient iterations. As pointed out by Hansen (1998), the number of iterations plays a role similar to a trade-off parameter.

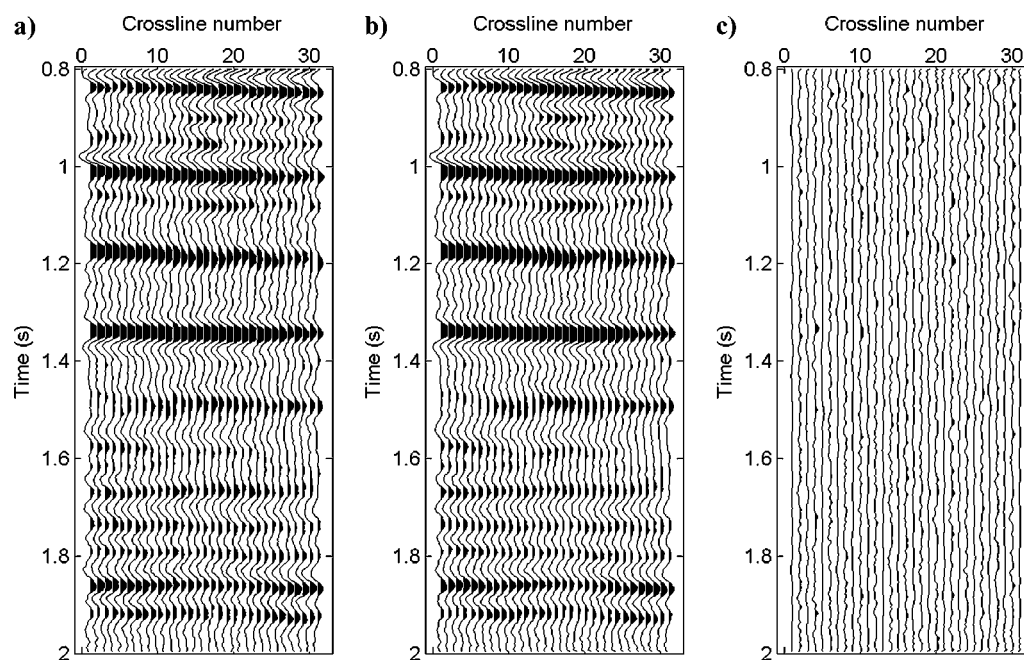


Figure 8. (a) Original data along inline 39 (line A, Figure 7b). (b) Reconstructed data using the MWNI method. (c) Reconstruction error.

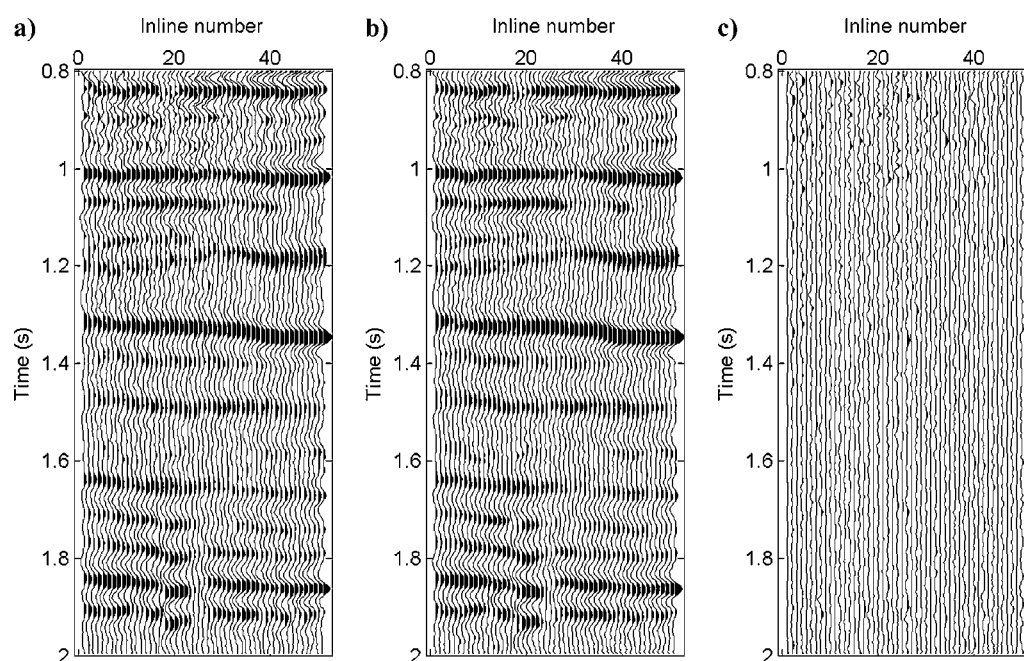


Figure 9. (a) Original data along crossline 19 (line B, Figure 7b). (b) Reconstructed data using the MWNI method. (c) Reconstruction error.

Consequently, by truncating the number of iterations, additive noise can be attenuated. The computational cost of the method makes it attractive for multidimensional interpolation.

Fourier interpolation methods can handle crossing events in as much as the data are not aliased. Although we did not show numerical results highlighting the interpolations with conflicting dips, our method may not be able to handle multiple crossing events if the data are aliased. This is significant because seismic data interpolation often involves spatially aliased data and multiple crossing events.

ACKNOWLEDGMENTS

The Signal Analysis and Imaging Group at the University of Alberta would like to acknowledge financial support from the following companies: Geo-X Ltd., Encana Ltd., Veritas Geoservices, and the Schlumberger Foundation. This research has also been supported by the Natural Sciences and Engineering Research Council of Canada and the Alberta Department of Energy.

We also appreciate the valuable comments and suggestions from the reviewers of *Geophysics* and Assistant Editor Yonghe Sun.

REFERENCES

- Bingham, C., M. D. Godfrey, and J. W. Tukey, 1967, Modern techniques of power spectrum estimation: *IEEE Transactions on Audio and Electroacoustics*, **15**, No. 2, 56–66.
- Cabrera, S. D., and T. W. Parks, 1991, Extrapolation and spectrum estimation with iterative weighted norm modification: *IEEE Transactions in Signal Processing*, **39**, 842–850.
- Cary, P. W., 1997, 3-D stacking of irregularly sampled data by wavefield reconstruction: 67th Annual International Meeting, SEG, Expanded Abstracts, 1104–1107.
- Claerbout, J. F., 1992, *Earth soundings analysis: Processing versus inversion*: Blackwell Scientific Publications, Inc.
- Davis, P. J., 1979, *Circulant matrices*: John Wiley & Sons, Inc.
- Duijndam, A. J. W., M. Schonewille, and K. Hindriks, 1999, Reconstruction of seismic signals, irregularly sampled along one spatial direction: *Geophysics*, **64**, 524–538.
- Hansen, P. C., 1998, Rank-deficient and discrete ill-posed problems: Numerical aspects of linear inversion: *SIAM Monographs on Mathematical Modeling and Computation* v. 4.
- Herrmann, P., T. Mojesky, M. Magesan, and P. Hugonnet, 2000, De-aliased, high-resolution Radon transforms: 70th Annual International Meeting, SEG, Expanded Abstracts, 1953–1956.
- Hestenes, M. R., 1975, Pseudoinverse and conjugate gradients: *Association for Computing Machinery*, **18**, No. 1, 40–43.
- Hindriks, K., A. J. W. Duijndam, and M. A. Schonewille, 1997, Reconstruction of two-dimensional irregularly sampled wavefields: 67th Annual International Meeting, SEG, Expanded Abstracts, 1163–1166.
- Hugonnet, P., P. Herrmann, and C. Ribeiro, 2001, High resolution Radon—A review: 63rd Meeting: European Association of Exploration Geophysicists, Extended Abstracts, Session IM-2.
- Jain, A. K., and S. Ranganath, 1981, Extrapolation algorithms for discrete signals with application in spectrum estimation: *IEEE Transactions in Acoustics, Speech and Signal Processing*, **29**, 830–845.
- Nichols, D., 1997, A simple example of a null space and how to modify it: Stanford Exploration Project Report, **82**, 182–192.
- Ronen, J., 1987, Wave-equation trace interpolation: *Geophysics*, **52**, 973–984.
- Sacchi, M. D., and T. J. Ulrych, 1996, Estimation of the discrete Fourier transform, a linear inversion approach: *Geophysics*, **61**, 1128–1136.
- Sacchi, M. D., T. J. Ulrych, and C. Walker, 1998, Interpolation and extrapolation using a high-resolution discrete Fourier transform: *IEEE Transactions in Signal Processing*, **46**, 31–38.
- Shuey, R. T., 1987, A simplification of the Zoeppritz equations: *Geophysics*, **50**, 993–1014.
- Spitz, S., 1991, Seismic trace interpolation in the F-X domain: *Geophysics*, **56**, 785–794.
- Strang, G., 1986, *Introduction to applied mathematics*: Wellesley-Cambridge Press.
- Zwartjes, P. M., and A. J. W. Duijndam, 2000, Optimizing reconstruction for sparse spatial sampling: 70th Annual International Meeting, SEG, Expanded Abstracts, 2162–2165.